NANO LETTERS

pubs.acs.org/NanoLett

Letter

Generic Orbital Design of Higher-Order Topological Quasicrystalline Insulators with Odd Five-Fold Rotation Symmetry

Huaqing Huang,* Jiahao Fan, Dexin Li, and Feng Liu*

Cite This: *Nano Lett.* 2021, 21, 7056−7062

Read Online

ACCESS | Metrics & More | Article Recommendations | Supporting Information

ABSTRACT: In addition to crystals, topological phases in quasicrystals and disorder systems have drawn increasing attention lately. Here, we propose a generic double band-inversion mechanism underlying the higher-order topological phase in quasicrystals, that is.,"higher-order topological quasicrystalline insulator" (HOTQI), which exploits local atomic orbital and lattice symmetries. It is generally applicable to both quasicrystals and crystals with either odd-rotational (OR) or even-rotational symmetry (ERS), different from previous HOTI mechanisms whose applicability is limited by symmetry types. The HOTQI is characterized by topological corner states at the nonordinary corners of pentagonal (octagonal) samples of five-fold (eight-fold) quasicrystals, which violate the translational invariance and ordinary crystalline symmetries. The role of quasicrystalline symmetry, the robustness against symmetry breaking, and possible experimental realizations are discussed. Our findings not only provide a concrete example of HOTQIs that is incompatible with classical crystallographic symmetry but also offer useful guidance to the search of higher-order topological materials and metamaterials.

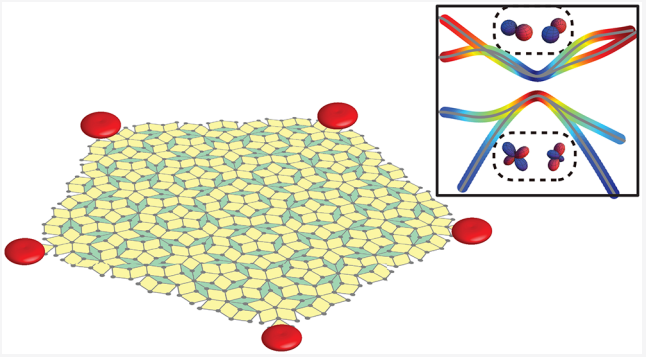

KEYWORDS: *higher-order topological insulator, quasicrystal, five-fold rotation symmetry, double band inversion*

Topological insulators, which are characterized by an insulating bulk and topologically protected metallic surface or edge states, have attracted considerable interest and have been comprehensively explored in the last two decades.[1,2] The recent discovery of higher-order topological insulators (HOTIs) has revived interest in the hidden electronic topology of the previously mistaken topologically "trivial" insulators without gapless boundary states in the reduced dimension.[3−7] A HOTI in n-dimension (nD) has a gapped bulk and $(n-1)$-dimensional boundary, but the gapless states emerge at lower dimensional boundaries, for example, the 0D corner of a 2D insulator. Specifically, a novel fractional quantization of a corner charge can be achieved in 2D rotation-symmetric HOTIs due to the mismatch between the number of electrons required to simultaneously satisfy charge neutrality and the crystal symmetry (also known as filling anomaly).[8] As a new extension of topological insulators, a variety of theoretical models have been proposed for HOTIs. Moreover, the material realization of HOTIs was explored in crystalline solids[9−18] as well as in artificial systems, such as photonic[19,20] or acoustic[21−24] metamaterials, ultracold atoms,[25] and even topolectrical circuits.[26−28]

Inspired by the rapid progress of HOTIs in crystalline systems, the study of higher-order topology has lately extended to quasicrystals which lack translation symmetry but contain crystallographic forbidden symmetries, such as the five-fold and eight-fold rotation symmetries. One of the prevailing mechanisms for higher-order topological phases is to gap out 1D lower boundary modes of conventional (first-order) topological phases in a nontrivial way, so that Dirac-mass domain walls form at intersections between adjacent boundaries. However, this mechanism is so far developed only for crystals or quasicrystals with ERS.[29,30] For ORS in crystals, that is, the C_3 symmetry as in a Kagome lattice, HOTIs can be realized by introducing a "breathing" structure[5,8,19,22,23,31] in which an imbalance between inter- and intracell hoppings is introduced to create a 2D analog of the Su−Schriffer−Heeger (SSH) model.[32] However, this model is not extendable to quasicrystals without translational symmetry. Thus, it remains unknown whether higher-order topology can exist in quasicrystals with C_5 ORS, which is the characteristic symmetry of the first experimentally discovered quasicrystal.[33] It is worth noting that the first-order topology does exist in C_5 quasicrystals.[34−36]

Received: July 9, 2021
Revised: August 2, 2021
Published: August 5, 2021

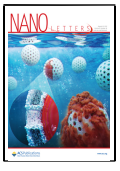

https://doi.org/10.1021/acs.nanolett.1c02661
Nano Lett. 2021, 21, 7056−7062

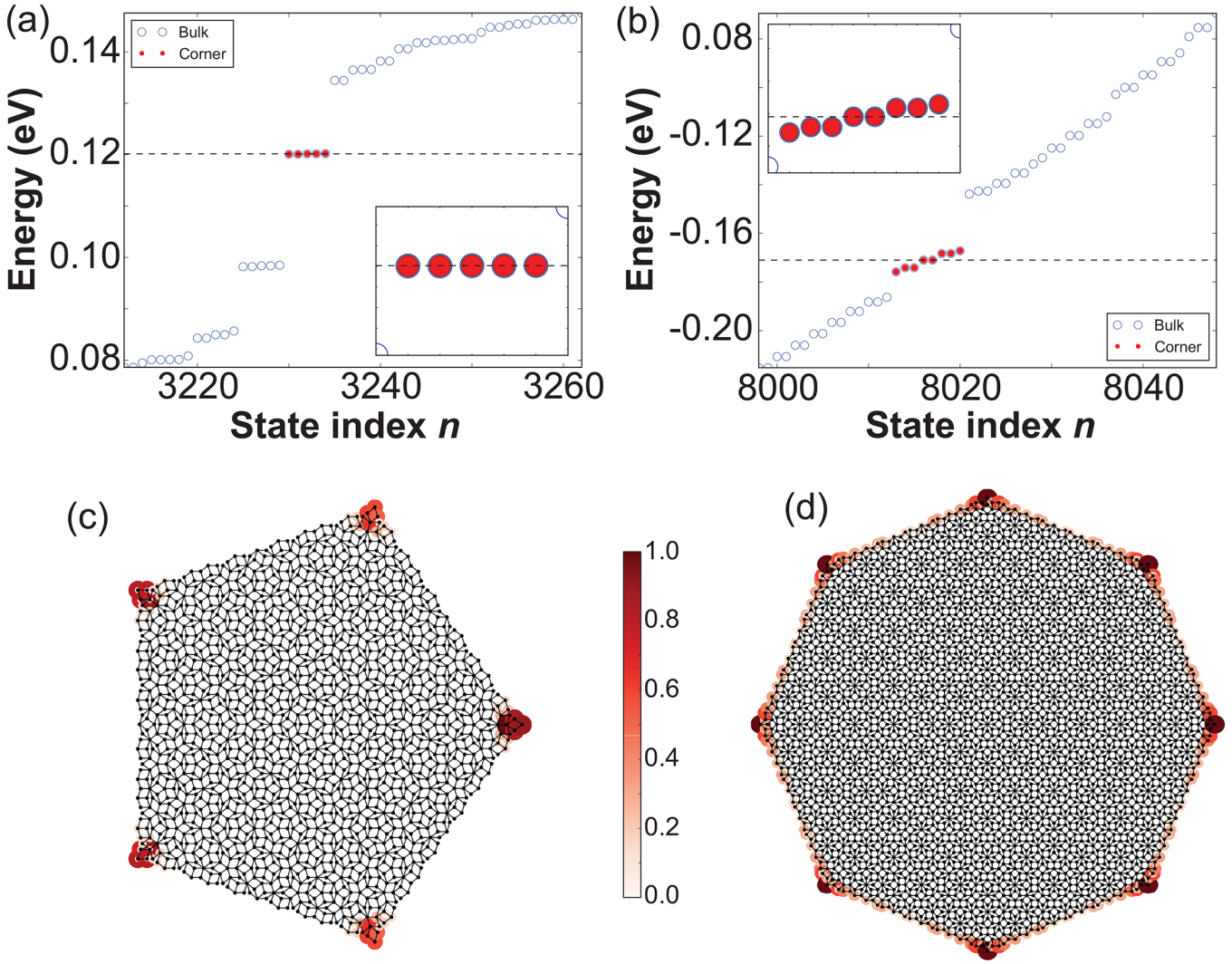

Figure 1. Higher-order topological quasicrystalline insulators. (a,b) Energy spectrum of a finite symmetric sample of (a) pentagonal and (b) octagonal quasicrystals. Insets show the zoomed-in plots of the spectrum around the Fermi level where corner states are marked in red. (c,d) The spatial charge distributions of corner states in (c) pentagonal and (d) octagonal quasicrystals. The color bar is proportional to the local charge density.

In this work, we propose a general mechanism for the realization of HOTQIs with topologically protected corner states, which is compatible with both ER (e.g., C_8) and OR (e.g., C_5) quasicrystalline symmetries. On the basis of real quasicrystals with atomic orbitals, the nontrivial topology of HOTQIs is shown to stem from a double band inversion between $p_x \pm ip_y$ and $d_{x^2-y^2} \pm id_{xy}$ orbital-derived states. We show that the HOTQI with topological corner states can be distinguished from trivial states by tracing the quasicrystalline rotational eigenvalues of occupied states. Moreover, we demonstrate that the proposed double band-inversion mechanism for achieving higher-order topology can be extended to other types of orbitals with different angular momenta and other lattices with different symmetries. Because our proposed HOTQIs do not require strong spin−orbit coupling (SOC), it is expected they can be realized in molecular crystals where SOC is negligibly weak as well as photonic and phononic metamaterials which are intrinsic spinless systems.

RESULTS AND DISCUSSION

The calculated results of a particular realization of the HOTQI in a Penrose-type C_5 quasicrystal and an Ammann−Beenker-type C_8 quasicrystal are presented in Figure 1. It is found that the finite pentagonal sample of the Penrose-type quasicrystal shows five states at the Fermi level which are separated from all other states, as displayed in Figure 1a. In Figure 1c, we plotted the spatial charge distribution of these states. Remarkably, these states are well localized at five corners of the pentagonal sample, that is, they correspond to isolated corner states. Moreover, we found two of the five corner states are occupied at half-filling of the whole spectrum, thus 2/5 electron charge localized at each corner is realized, leading to a fractionalized charge distribution. For the Ammann−Beenker-type quasicrystal, eight corner states, as expected, occur around the Fermi level (see Figure 1b). It is noted that there exists a slight finite-size-effect-induced energy splitting for these corner states, which is exponentially suppressed with the increasing sample size. As shown in Figure 1d, these states mainly distribute at the corners of the octagonal sample. There is a fractional charge of 5/8 electron per corner at half-filling of the spectrum.

https://doi.org/10.1021/acs.nanolett.1c02661
Nano Lett. 2021, 21, 7056−7062

It is worth noting that the total number (five or eight) of corner states in the two systems are exactly compatible with their unique C_5 and C_8 quasicrystalline symmetry, respectively, demonstrating the realization of HOTQIs in quasicrystals with ORS as well as ERS.

Physically, the p−d band inversion has played a key role in the realization of HOTQIs. However, due to the lack of translational symmetry, the Bloch theorem does not apply to quasicrystals, which hinders a direct visualization of the double band inversion from orbital-resolved band structures. On the other hand, it is possible to generate a sequence of periodic lattices with growing unit cells that converge to the infinite quasicrystal in a systemic way according to the quaiscrystal tiling approximants (see Supporting Information and Figures S1 and S2). Taking the simplest approximant of the octagonal quasicrystal, the square lattice, as an example, it is found that a double band inversion between the p- and d-orbital dominated bands takes place around the central Γ-point of the Brillouin zone (Figure 2a), signifying the nontrivial electronic topology

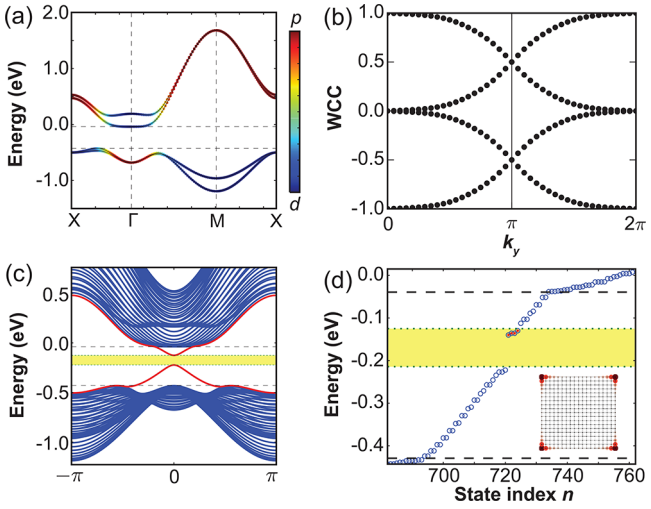

Figure 2. Higher-order topological state in the simplest approximant, a square lattice. (a) Orbital-resolved bulk band structure where a p−d band inversion occurs around Γ. (b) The evolution of Wannier charge center as a function of k_y. (c) Band structure of a nanoribbon where topological edge states (the red lines) are gapped out. (d) Energy spectrum of a finite square sample where topological corner states (red dots) appear within the edge-gap region (yellow area). The inset shows the spatial charge distribution of corner states.

in this system. Similar p−d band inversion also occurs in all other periodic approximants with more complicated unit cells (see Figures S3 and S4). In Figure 2b, we plotted the evolution of Wannier charge centers (WCCs) for occupied bands and found that the WCCs switch partners during the evolution, which is similar to that of the time-reversal (TR) symmetry-protected quantum spin Hall (QSH) states.[37] In fact, the linear combination of orbitals with positive and negative angular momentum (magnetic quantum number) can be regarded as the up and down pseudospin states (see Supporting Information), respectively, that is

$$\mathrm{p}_{\pm} = \frac{1}{\sqrt{2}}(\mathrm{p}_x \pm i\mathrm{p}_y), \quad \mathrm{d}_{\pm} = \frac{1}{\sqrt{2}}(\mathrm{d}_{x^2-y^2} \pm i\mathrm{d}_{xy}) \tag{1}$$

On the basis of these pseudospin states, the double band inversion can be described by an effective $k.p$ Hamiltonian resembling the Bernevig−Hughes−Zhang (BHZ) model, which was originally proposed for the QSH state in HgTe/CdTe quantum wells.[38]

However, different from the BHZ model, pseudospins instead of real spins are used, so that SOC, which plays an important role in the realization of QSH states, is not required in the present model. Moreover, a pseudo-TR symmetry $\mathcal{T}$ with $\mathcal{T}^2 = -1$ is satisfied only for the bulk with fine-tuned parameters (see the Supporting Information). This can also be seen from the fact that only valence-band states are degenerate at Γ, while conduction-band states are not (i.e., a pseudo-Kramers degeneracy does not exist), as shown in Figure 2a. Therefore, different from the QSH effect that supports gapless helical edge states protected by TR, the edge states of our model are generally gapped due to the breakage of the pseudo-TR symmetry that mixes the two pseudospin channels (see Figure 2c). Remarkably, by further studying the energy spectrum of the finite square sample, we found that four states (marked as red dots) appear within the edge-gap region (yellow area) and are localized at four corners of the sample, as shown in Figure 2d. We further calculated the quadrupole moment Q_{xy}, which is a natural topological invariant to characterize 2D HOTIs.[16,39] The numerical calculation shows that the corner states appear when $Q_{xy} = 1/2$, confirming the nontrivial higher-order topology in these systems. We emphasize that the same HOTIs exist in a series of periodic approximants with increasing lattice size as long as p−d band inversions occur, indicating that the higher-order topological characteristics should also appear in infinite quasicrystals.

Although the periodic approximant provides a heuristic picture to illustrate the underlying mechanism of the higher-order topology, it is more revealing to explicitly analyze the essential feature of HOTQIs from the symmetry-based argument. The most unique symmetry of the above quasicrystals is the n-fold rotation C_n (n = 5, 8) which is strictly prohibited in crystals. In addition, the quasicrystals also have vertical mirror symmetries M_v, which are useful in the analysis of topological corner states, as we show below.

According to the character tables of C_{5v} and C_{8v} point groups as shown in Tables 1 and 2, the doubly degenerate orbitals $\mathrm{p}_{\pm1}$ and $\mathrm{d}_{\pm2}$ belong to the 2D irreducible representation E_1 and E_2, respectively, and therefore are properly chosen as bases for the realization of double band inversion. The nontrivial higher-order topology is revealed by a corner-induced filling anomaly,[8,40,41] that is, an obstruction to simultaneously satisfying charge neutrality and preserving the lattice symmetry in the presence of corners. For trivial states without double band inversion, the occupied states can be adiabatically connected to the atomic limit. In contrast, when the double band inversion occurs in $C_{5/8}$-symmetric systems, the electronic Wannier centers of occupied states are no longer consistent with atomic positions, giving rise to the topological corner charges.

Table 1. Character Table for the C_{5v} Point Group

C_{5v}	E	$2C_5$	$2C_5^2$	$5\sigma_v$	bases
A_1	1	1	1	1	p_0; d_0
A_2	1	1	1	−1	$\mathrm{h}_5 - \mathrm{h}_{-5}$
E_1	2	$2\cos(2\pi/5)$	$2\cos(4\pi/5)$	0	$\mathrm{p}_{\pm1}$; $\mathrm{d}_{\pm1}$
E_2	2	$2\cos(4\pi/5)$	$2\cos(2\pi/5)$	0	$\mathrm{d}_{\pm2}$; $\mathrm{f}_{\pm2}$; $\mathrm{f}_{\pm3}$

https://doi.org/10.1021/acs.nanolett.1c02661
Nano Lett. 2021, 21, 7056−7062

Table 2. Character Table for the C_{8v} Point Group

C_{8v}	E	$2C_8$	$2C_4$	$2C_8^3$	C_2	$4\sigma_v$	$4\sigma_d$	bases
A_1	1	1	1	1	1	1	1	p_0; d_0
A_2	1	1	1	1	1	−1	−1	
B_1	1	−1	1	−1	1	1	−1	$g_4 + g_{-4}$
B_2	1	−1	1	−1	1	−1	1	$g_4 - g_{-4}$
E_1	2	$2\cos(\pi/4)$	0	$-2\cos(\pi/4)$	−2	0	0	$p_{\pm1}$; $d_{\pm1}$
E_2	2	0	−2	0	2	0	0	$d_{\pm2}$; $f_{\pm2}$
E_3	2	$-2\cos(\pi/4)$	0	$2\cos(\pi/4)$	−2	0	0	$f_{\pm3}$; $g_{\pm3}$

The HOTQIs can be distinguished from trivial states by considering the eigenvalues of rotation symmetry. For example, the C_8 operator is

$$\hat{C}_8 = \exp\left(-i\frac{\pi}{4}\sigma\right)R \tag{2}$$

where σ is the rotation matrix in the orbital space, and R is an orthogonal matrix permuting the sites of the quasicrystal to rotate the whole system by an angle of $\pi/4$. The eigenvalues of $\hat{C}_8$ are $\omega_p = e^{i\pi p/4}$, $(p = 0, ..., 7)$. Since $p_{\pm1}$ and $d_{\pm2}$ dominate states belonging to different ω_p, the index $\chi^{(8)} = (n_{\pm1}, n_{\pm2})$ determines the HOTQI arising from the p−d band inversion for any C_{8v}-symmetric quasicrystals. Here $n_{\pm p}$ is the number of states with the rotational eigenvalue ω_p or ω_{8-p} in the occupied subspace. For the C_{8v}-symmetric quasicrystal, a $\chi^{(8)}$, different from $\chi_0^{(8)}$ of the trivial atomic limit, signals an obstructed atomic limit, implying the existence of topological corner charges. Similarly, a index $\chi^{(5)}$ can be proposed to determine HOTQIs in C_{5v}-symmetric quasicrystals.

The corner states can also be understood as the domain-wall states from the boundary perspective. Let us first analyze the manifestation of the HOTQI in eight-fold quasicrystals. As elucidated above, the band-inversion-induced edge states are generally gapped due to the "intrinsic" pseudo-TR breaking. Such a gapped edge state can be captured by a 1D Dirac model with a mass term

$$H_{\text{edge}} = -iv(l)\partial_l\sigma_z + m(l)\sigma_x \tag{3}$$

where l is the real-space coordinate along the boundary, and σ_x and σ_z are Pauli matrices for pseudospin. A 0D bound state should arise as the topological domain-wall state at the intersection between two edges with opposite mass terms. Crucially, the mass term is odd under M_v (see Supporting Information Section S2). Hence, adjacent edges related by M_v would generally have opposite signs of the mass term, ensuring the existence of corner states at the intersection between them.[6,42−44] In a symmetric octagonal sample of the C_8 quasicrystal, corners on M_v-invariant lines are also connected by C_8 symmetry. Therefore, the mass terms of edge states change signs alternatively across the whole perimeter of the sample (see Figure 3a). This gives rise to a total of eight topological corner states around the Fermi level, as shown in Figure 1b.

The above analysis shows a sufficient condition: a 0D bound state exists at the corner where two M_v-related edges meet. The argument relies on an alternating sign of the mass term at the boundary, so it seemed only applicable to ERS corners but not ORS corners, that is, the symmetry of pentagonal sample of C_5 quasicrystals. However, based on an artificial transformation process of the boundary, one can validate the existence of corner states at ORS corners. Hypothetically, let us start with a decagonal sample, as shown in Figure 3b. Similar to the aforementioned analysis, 10 ER corners locate on 5 vertical mirror planes, which separate mirror-related edges and host topological corner states. Assuming these 10 corner states split into two groups with different energies due to distinct local atomic environments (see different colors in Figure 3b). Now, let us gradually move the boundary to form a pentagonal sample, that is, smoothly moving alternative 5 of the 10 corners toward the center without breaking M_v. Then, at the end of reaching Figure 3c, the edges of the pentagonal sample become mirror symmetric, so that the mass term is not necessarily generated along the edge and five bound states merge into bulk continuum and annihilate, leaving only five corner states that persist at the Fermi level.[42−44] Although there can be different number and distribution of corner states in the sample, we emphasize that the corner-induced filling anomaly is still valid, which guarantees the existence of at least one set of five-fold degenerate states localized at corners of C_{5v}-symmetric quaiscrystals.[8,40,41]

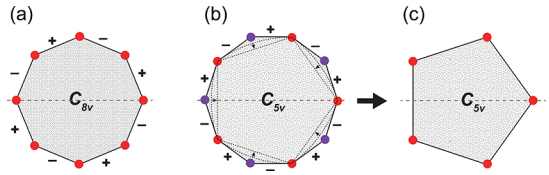

Figure 3. Schematic illustration of topological corner states in quasicrystals. (a,b) The distribution of edge mass terms and corner states across the perimeter of (a) eight-fold and (b) five-fold quasicrystal samples. (c) By moving the alternative 5 of the 10 corners to form a pentagonal sample, 5 corner states move away from the Fermi level. Corner states with different energy are marked by different color.

Fundamentally, the HOTQI is attributed to the double band inversion mechanism, but the number and type of corner states depend on the properties of boundary (i.e., the lattice termination). According to the topological classification of Geier et al.,[42] such corner states are considered "extrinsic", as they are not merely subjected to the exact quasicrystalline symmetry of the entire sample and may be removed by decorating the boundary. However, we found that they are quite robust against weak perturbation that breaks the lattice symmetry, as long as the bulk and edge gaps are preserved and the original double band inversion can be identified. Our calculation shows that topological corner states remain robustly if M_v and/or C_n symmetries were weakly broken by local twisting or distortion (Figures S13−S15). Moreover, it is found that corner states even persist in asymmetric samples when one or more corners are removed (Figures S16 and S23).

We note that the p−d band inversion was previously proposed to achieve topological photonic crystals in 2D deformed honeycomb lattices.[45] In those systems, effective $p_{x,y}$

https://doi.org/10.1021/acs.nanolett.1c02661
Nano Lett. 2021, 21, 7056−7062

and d_{xy,x^2-y^2} basis are represented by "metamolecular orbitals" in honeycomb unitcell. The double band inversion is realized by tuning the intra- and intermetamolecular coupling. Following this idea, various metamaterial structures with C_{6v} symmetry have been proposed to realize photonic and acoustic topological states.[46−55] Here, we show that actually the p−d band inversion mechanism is not restricted to the C_{6v} symmetry; it is also applicable to other crystalline systems with C_{2v}, C_{3v}, and C_{4v} symmetries (Figures S17−S19) and even quasicrystals with C_{5v} and C_{8v} symmetries, as elaborated above. More importantly, we emphasize that the prevailing band inversion mechanism is not limited to $p_{\pm1}$ and $d_{\pm2}$ orbitals, and other pairs of bands such as d−d, d−f, and f−g can also be employed for the inversion to achieve higher-order topological states, as long as both bulk and edge spectrum can be gapped out. For example, we have demonstrated that a double band inversion between $d_{\pm1}$ and $f_{\pm2}$ orbitals would also induce higher-order topological phases, while a double band inversion between $d_{\pm1}$ and $d_{\pm2}$ is only valid for structurally buckled lattices because the in-plane mirror symmetry of planar lattices forbids interactions between these orbitals (see the Supporting Information and Figures S21−S25).

Our proposed orbital-designed scheme for achieving higher-order topological phases is expected to be experimentally realizable in different ways. First, as high-angular-momentum molecular orbitals (e.g., d, f, and g orbitals) can be derived from sp-atomic orbitals, higher-order topological states with double band inversions between selected orbitals are realizable in covalent/metal−organic frameworks or molecular crystals[56] on crystalline/quasicrystalline template substrates via molecular self-assembly or atomic manipulation.[31,57−59] Moreover, as the role of pseudospin is played by the angular momentum of wave functions involved in the double band inversion, the electron spin, SOC, and even single atomic orbital basis are not essentially required. The prerequisite for higher-order topology is therefore rationalized to a simple double band inversion between states with the same symmetry as foregoing orbitals. For example, recently, topological corner modes are realized in pentagonal domains of elastic phononic crystals based on the p−d double band inversion with aperiodic modulated Dirac vortices.[60] Hence, with properly designed basic building blocks, one may realize the proposed HOTQIs in various metamaterials, such as photonic or phononic crystals, ultracold atoms, microwave or electrical circuits, and classical mechanical or acoustic metamaterials.[61,62] Thus, we expect that our proposal would draw immediate experimental attention.

CONCLUSION

We have proposed the realization of HOTQIs by exploiting a generally designed double band inversion mechanism. HOTQIs possessing five (eight) topological corner states in pentagonal (octagonal) samples of five-fold (eight-fold) quasicrystals are demonstrated, which is compatible with quasicrystalline symmetries but absent in crystals. In addition to the specific examples elucidated, the essential double band inversion mechanism necessitating the higher-order topology is also extendable to other types of orbitals and lattice symmetries, providing practical guidance toward HOTQIs in real materials as well as metamaterials. Furthermore, we also expect that our proposed scheme is applicable to 3D structures which may open additional exciting possibilities. For example, by stacking 2D HOTQIs, one may realize 3D higher-order topological quasicrystals hosting topological corner states, gapless hinge modes, or hinge Fermi arcs.[63−65]

METHODS

We consider a spinless tight-binding model for 2D quasicrystal lattices with p_x, p_y, d_{xy} and $d_{x^2-y^2}$ orbitals on each site. The Hamiltonian is given by

$$H = \sum_{i\alpha} \epsilon_\alpha c_{i\alpha}^\dagger c_{i\alpha} + \sum_{\langle i\alpha, j\beta\rangle} t_{\alpha\beta}(\mathbf{r}_{ij}) c_{i\alpha}^\dagger c_{j\beta} \tag{4}$$

where $c_{i\alpha}^\dagger$ and $c_{i\alpha}$ are electron creation and annihilation operators on the $\alpha(=p_x, p_y, d_{xy}, d_{x^2-y^2})$ orbital at the ith site, respectively. ϵ_α is the on-site energy of the α orbital. For simplicity, we assume that p_x and p_y (d_{xy} and $d_{x^2-y^2}$) orbitals have the same on-site energy ϵ_p (ϵ_d). $t_{\alpha\beta}(\mathbf{r}_{ij})$ are the Slater−Koster parametrized hopping integrals which depend on the orbital type (α and β) and the directional cosines of the intersite vector $\mathbf{r}_{ij} = \mathbf{r}_i - \mathbf{r}_j$.[66,67] Since we are particularly interested in the double band inversion between p and d orbitals, electron occupation is fixed at half filling in all calculations. We emphasize that the explicit form of the Hamiltonian H is only determined by orbital and lattice symmetries to capture the essential feature of the p−d band inversion so that the model is generally applicable to other spinless or SOC-free systems.

ASSOCIATED CONTENT

Supporting Information

The Supporting Information is available free of charge at https://pubs.acs.org/doi/10.1021/acs.nanolett.1c02661.

Numerical results of quasicrystals; theoretical analysis; higher-order topology induced by other types of band inversion (PDF)

AUTHOR INFORMATION

Corresponding Authors

Huaqing Huang − *School of Physics, Peking University, Beijing 100871, China; Center for High Energy Physics, Peking University, Beijing 100871, China; Collaborative Innovation Center of Quantum Matter, Beijing 100871, China;* orcid.org/0000-0002-0283-8603; Email: huaqing.huang@pku.edu.cn

Feng Liu − *Department of Materials Science and Engineering, University of Utah, Salt Lake City, Utah 84112, United States;* orcid.org/0000-0002-3701-8058; Email: fliu@eng.utah.edu

Authors

Jiahao Fan − *School of Physics, Peking University, Beijing 100871, China*

Dexin Li − *School of Physics, Peking University, Beijing 100871, China*

Complete contact information is available at: https://pubs.acs.org/10.1021/acs.nanolett.1c02661

Notes

The authors declare no competing financial interest.

https://doi.org/10.1021/acs.nanolett.1c02661
Nano Lett. 2021, 21, 7056−7062

■ ACKNOWLEDGMENTS

H.H., J.F., and D.L. were supported by the National Natural Science Foundation of China (Grant 12074006) and the start-up fund from Peking University. H.H. was also partially supported and F.L. was fully supported by U.S. DOE-BES (Grant DE-FG02-04ER46148). The computational resources were supported by the high-performance computing platform of Peking University, the CHPC at the University of Utah, and the NERSC at the Office of Science in the U.S. Department of Energy.

■ REFERENCES

(1) Hasan, M. Z.; Kane, C. L. Colloquium: Topological insulators. *Rev. Mod. Phys.* **2010**, *82*, 3045−3067.
(2) Qi, X.-L.; Zhang, S.-C. Topological insulators and superconductors. *Rev. Mod. Phys.* **2011**, *83*, 1057−1110.
(3) Benalcazar, W. A.; Bernevig, B. A.; Hughes, T. L. Quantized electric multipole insulators. *Science* **2017**, *357*, 61−66.
(4) Schindler, F.; Cook, A. M.; Vergniory, M. G.; Wang, Z.; Parkin, S. S.; Bernevig, B. A.; Neupert, T. Higher-order topological insulators. *Sci. Adv.* **2018**, *4*, No. eaat0346.
(5) Ezawa, M. Higher-Order Topological Insulators and Semimetals on the Breathing Kagome and Pyrochlore Lattices. *Phys. Rev. Lett.* **2018**, *120*, 026801.
(6) Langbehn, J.; Peng, Y.; Trifunovic, L.; von Oppen, F.; Brouwer, P. W. Reflection-Symmetric Second-Order Topological Insulators and Superconductors. *Phys. Rev. Lett.* **2017**, *119*, 246401.
(7) Song, Z.; Fang, Z.; Fang, C. $(d-2)$-Dimensional Edge States of Rotation Symmetry Protected Topological States. *Phys. Rev. Lett.* **2017**, *119*, 246402.
(8) Benalcazar, W. A.; Li, T.; Hughes, T. L. Quantization of fractional corner charge in C_n-symmetric higher-order topological crystalline insulators. *Phys. Rev. B: Condens. Matter Mater. Phys.* **2019**, *99*, 245151.
(9) Schindler, F.; Wang, Z.; Vergniory, M. G.; Cook, A. M.; Murani, A.; Sengupta, S.; Kasumov, A. Y.; Deblock, R.; Jeon, S.; Drozdov, I.; Bouchiat, H.; Guéron, S.; Yazdani, A.; Bernevig, B. A.; Neupert, T. Higher-order topology in bismuth. *Nat. Phys.* **2018**, *14*, 918.
(10) Yue, C.; Xu, Y.; Song, Z.; Weng, H.; Lu, Y.-M.; Fang, C.; Dai, X. Symmetry-enforced chiral hinge states and surface quantum anomalous hall effect in the magnetic axion insulator bi 2−x sm x se 3. *Nat. Phys.* **2019**, *15*, 577−581.
(11) Xu, Y.; Song, Z.; Wang, Z.; Weng, H.; Dai, X. Higher-Order Topology of the Axion Insulator $EuIn_2As_2$. *Phys. Rev. Lett.* **2019**, *122*, 256402.
(12) Zhang, R.-X.; Wu, F.; Das Sarma, S. Möbius Insulator and Higher-Order Topology in $MnBi_{2n}Te_{3n+1}$. *Phys. Rev. Lett.* **2020**, *124*, 136407.
(13) Wang, Z.; Wieder, B. J.; Li, J.; Yan, B.; Bernevig, B. A. Higher-Order Topology, Monopole Nodal Lines, and the Origin of Large Fermi Arcs in Transition Metal Dichalcogenides XTe_2 (X = Mo, W). *Phys. Rev. Lett.* **2019**, *123*, 186401.
(14) Sheng, X.-L.; Chen, C.; Liu, H.; Chen, Z.; Yu, Z.-M.; Zhao, Y. X.; Yang, S. A. Two-Dimensional Second-Order Topological Insulator in Graphdiyne. *Phys. Rev. Lett.* **2019**, *123*, 256402.
(15) Lee, E.; Kim, R.; Ahn, J.; Yang, B.-J. Two-dimensional higher-order topology in monolayer graphdiyne. *npj Quantum Mater.* **2020**, *5*, 1−7.
(16) Liu, B.; Zhao, G.; Liu, Z.; Wang, Z. Two-Dimensional Quadrupole Topological Insulator in γ-Graphyne. *Nano Lett.* **2019**, *19*, 6492−6497.
(17) Park, M. J.; Kim, Y.; Cho, G. Y.; Lee, S. Higher-Order Topological Insulator in Twisted Bilayer Graphene. *Phys. Rev. Lett.* **2019**, *123*, 216803.
(18) Liu, B.; Xian, L.; Mu, H.; Zhao, G.; Liu, Z.; Rubio, A.; Wang, Z. F. Higher-Order Band Topology in Twisted Moiré Superlattice. *Phys. Rev. Lett.* **2021**, *126*, 066401.
(19) Mittal, S.; Orre, V. V.; Zhu, G.; Gorlach, M. A.; Poddubny, A.; Hafezi, M. Photonic quadrupole topological phases. *Nat. Photonics* **2019**, *13*, 692−696.
(20) El Hassan, A.; Kunst, F. K.; Moritz, A.; Andler, G.; Bergholtz, E. J.; Bourennane, M. Corner states of light in photonic waveguides. *Nat. Photonics* **2019**, *13*, 697−700.
(21) Serra-Garcia, M.; Peri, V.; Süsstrunk, R.; Bilal, O. R.; Larsen, T.; Villanueva, L. G.; Huber, S. D. Observation of a phononic quadrupole topological insulator. *Nature* **2018**, *555*, 342−345.
(22) Xue, H.; Yang, Y.; Gao, F.; Chong, Y.; Zhang, B. Acoustic higher-order topological insulator on a kagome lattice. *Nat. Mater.* **2019**, *18*, 108−112.
(23) Ni, X.; Weiner, M.; Alu, A.; Khanikaev, A. B. Observation of higher-order topological acoustic states protected by generalized chiral symmetry. *Nat. Mater.* **2019**, *18*, 113−120.
(24) Zhang, X.; Wang, H.-X.; Lin, Z.-K.; Tian, Y.; Xie, B.; Lu, M.-H.; Chen, Y.-F.; Jiang, J.-H. Second-order topology and multidimensional topological transitions in sonic crystals. *Nat. Phys.* **2019**, *15*, 582−588.
(25) Pelegrí, G.; Marques, A. M.; Ahufinger, V.; Mompart, J.; Dias, R. G. Second-order topological corner states with ultracold atoms carrying orbital angular momentum in optical lattices. *Phys. Rev. B: Condens. Matter Mater. Phys.* **2019**, *100*, 205109.
(26) Peterson, C. W.; Benalcazar, W. A.; Hughes, T. L.; Bahl, G. A quantized microwave quadrupole insulator with topologically protected corner states. *Nature* **2018**, *555*, 346−350.
(27) Peterson, C. W.; Li, T.; Benalcazar, W. A.; Hughes, T. L.; Bahl, G. A fractional corner anomaly reveals higher-order topology. *Science* **2020**, *368*, 1114−1118.
(28) Imhof, S.; Berger, C.; Bayer, F.; Brehm, J.; Molenkamp, L. W.; Kiessling, T.; Schindler, F.; Lee, C. H.; Greiter, M.; Neupert, T.; Thomale, R. Topolectrical-circuit realization of topological corner modes. *Nat. Phys.* **2018**, *14*, 925−929.
(29) Varjas, D.; Lau, A.; Pöyhönen, K.; Akhmerov, A. R.; Pikulin, D. I.; Fulga, I. C. Topological Phases without Crystalline Counterparts. *Phys. Rev. Lett.* **2019**, *123*, 196401.
(30) Chen, R.; Chen, C.-Z.; Gao, J.-H.; Zhou, B.; Xu, D.-H. Higher-Order Topological Insulators in Quasicrystals. *Phys. Rev. Lett.* **2020**, *124*, 036803.
(31) Kempkes, S.; Slot, M.; van Den Broeke, J.; Capiod, P.; Benalcazar, W.; Vanmaekelbergh, D.; Bercioux, D.; Swart, I.; Smith, C. M. Robust zero-energy modes in an electronic higher-order topological insulator. *Nat. Mater.* **2019**, *18*, 1292−1297.
(32) Su, W. P.; Schrieffer, J. R.; Heeger, A. J. Solitons in Polyacetylene. *Phys. Rev. Lett.* **1979**, *42*, 1698−1701.
(33) Shechtman, D.; Blech, I.; Gratias, D.; Cahn, J. W. Metallic Phase with Long-Range Orientational Order and No Translational Symmetry. *Phys. Rev. Lett.* **1984**, *53*, 1951−1953.
(34) Huang, H.; Liu, F. Quantum Spin Hall Effect and Spin Bott Index in a Quasicrystal Lattice. *Phys. Rev. Lett.* **2018**, *121*, 126401.
(35) Huang, H.; Liu, F. Theory of spin Bott index for quantum spin Hall states in nonperiodic systems. *Phys. Rev. B: Condens. Matter Mater. Phys.* **2018**, *98*, 125130.
(36) Bandres, M. A.; Rechtsman, M. C.; Segev, M. Topological Photonic Quasicrystals: Fractal Topological Spectrum and Protected Transport. *Phys. Rev. X* **2016**, *6*, 011016.
(37) Soluyanov, A. A.; Vanderbilt, D. Computing topological invariants without inversion symmetry. *Phys. Rev. B: Condens. Matter Mater. Phys.* **2011**, *83*, 235401.
(38) Bernevig, B. A.; Hughes, T. L.; Zhang, S.-C. Quantum Spin Hall Effect and Topological Phase Transition in HgTe Quantum Wells. *Science* **2006**, *314*, 1757−1761.
(39) Liu, F.; Wakabayashi, K. Novel Topological Phase with a Zero Berry Curvature. *Phys. Rev. Lett.* **2017**, *118*, 076803.
(40) Watanabe, H.; Ono, S. Corner charge and bulk multipole moment in periodic systems. *Phys. Rev. B: Condens. Matter Mater. Phys.* **2020**, *102*, 165120.
(41) Takahashi, R.; Zhang, T.; Murakami, S. General corner charge formula in two-dimensional C_n-symmetric higher-order topological

https://doi.org/10.1021/acs.nanolett.1c02661
Nano Lett. 2021, 21, 7056−7062

insulators. *Phys. Rev. B: Condens. Matter Mater. Phys.* **2021**, *103*, 205123.
(42) Geier, M.; Trifunovic, L.; Hoskam, M.; Brouwer, P. W. Second-order topological insulators and superconductors with an order-two crystalline symmetry. *Phys. Rev. B: Condens. Matter Mater. Phys.* **2018**, *97*, 205135.
(43) Trifunovic, L.; Brouwer, P. W. Higher-Order Bulk-Boundary Correspondence for Topological Crystalline Phases. *Phys. Rev. X* **2019**, *9*, 011012.
(44) Trifunovic, L.; Brouwer, P. W. Higher-Order Topological Band Structures. Phys. *Phys. Status Solidi B* **2021**, *258*, 2000090.
(45) Wu, L.-H.; Hu, X. Scheme for Achieving a Topological Photonic Crystal by Using Dielectric Material. *Phys. Rev. Lett.* **2015**, *114*, 223901.
(46) Wu, L.-H.; Hu, X. Topological properties of electrons in honeycomb lattice with detuned hopping energy. *Sci. Rep.* **2016**, *6*, 24347.
(47) Kariyado, T.; Jiang, Y.-C.; Yang, H.; Hu, X. Counterpropagating topological interface states in graphene patchwork structures with regular arrays of nanoholes. *Phys. Rev. B: Condens. Matter Mater. Phys.* **2018**, *98*, 195416.
(48) Yang, Y.; Xu, Y. F.; Xu, T.; Wang, H.-X.; Jiang, J.-H.; Hu, X.; Hang, Z. H. Visualization of a Unidirectional Electromagnetic Waveguide Using Topological Photonic Crystals Made of Dielectric Materials. *Phys. Rev. Lett.* **2018**, *120*, 217401.
(49) Li, Y.; Sun, Y.; Zhu, W.; Guo, Z.; Jiang, J.; Kariyado, T.; Chen, H.; Hu, X. Topological LC-circuits based on microstrips and observation of electromagnetic modes with orbital angular momentum. *Nat. Commun.* **2018**, *9*, 4598.
(50) Shao, Z.-K.; Chen, H.-Z.; Wang, S.; Mao, X.-R.; Yang, Z.-Q.; Wang, S.-L.; Wang, X.-X.; Hu, X.; Ma, R.-M. A high-performance topological bulk laser based on band-inversion-induced reflection. *Nat. Nanotechnol.* **2020**, *15*, 67−72.
(51) He, C.; Ni, X.; Ge, H.; Sun, X.-C.; Chen, Y.-B.; Lu, M.-H.; Liu, X.-P.; Chen, Y.-F. Acoustic topological insulator and robust one-way sound transport. *Nat. Phys.* **2016**, *12*, 1124−1129.
(52) Zhang, Z.; Wei, Q.; Cheng, Y.; Zhang, T.; Wu, D.; Liu, X. Topological Creation of Acoustic Pseudospin Multipoles in a Flow-Free Symmetry-Broken Metamaterial Lattice. *Phys. Rev. Lett.* **2017**, *118*, 084303.
(53) Liu, F.; Deng, H.-Y.; Wakabayashi, K. Helical Topological Edge States in a Quadrupole Phase. *Phys. Rev. Lett.* **2019**, *122*, 086804.
(54) Xie, B.; Su, G.; Wang, H.-F.; Liu, F.; Hu, L.; Yu, S.-Y.; Zhan, P.; Lu, M.-H.; Wang, Z.; Chen, Y.-F. Higher-order quantum spin Hall effect in a photonic crystal. *Nat. Commun.* **2020**, *11*, 1−8.
(55) Lin, Z.-K.; Wu, S.-Q.; Wang, H.-X.; Jiang, J.-H. Higher-Order Topological Spin Hall Effect of Sound. *Chin. Phys. Lett.* **2020**, *37*, 074302.
(56) Cui, B.; Huang, B.; Li, C.; Zhang, X.; Jin, K.-H.; Zhang, L.; Jiang, W.; Liu, D.; Liu, F. Creation of half-metallic *f*-orbital Dirac fermion with superlight elements in orbital-designed molecular lattice. *Phys. Rev. B: Condens. Matter Mater. Phys.* **2017**, *96*, 085134.
(57) Collins, L. C.; Witte, T. G.; Silverman, R.; Green, D. B.; Gomes, K. K. Imaging quasiperiodic electronic states in a synthetic Penrose tiling. *Nat. Commun.* **2017**, *8*, 15961.
(58) Zollner, E. M.; Schenk, S.; Förster, S.; Widdra, W. C_{60} adsorption on a dodecagonal oxide quasicrystal. *Phys. Rev. B: Condens. Matter Mater. Phys.* **2019**, *100*, 205414.
(59) Kalashnyk, N.; Ledieu, J.; Gaudry, É.; Cui, C.; Tsai, A.-P.; Fournée, V. Building 2D quasicrystals from 5-fold symmetric corannulene molecules. *Nano Res.* **2018**, *11*, 2129−2138.
(60) Wu, X.; Meng, Y.; Hao, Y.; Zhang, R.-Y.; Li, J.; Zhang, X. Topological Corner Modes Induced by Dirac Vortices in Arbitrary Geometry. *Phys. Rev. Lett.* **2021**, *126*, 226802.
(61) Kim, M.; Jacob, Z.; Rho, J. Recent advances in 2D, 3D and higher-order topological photonics. *Light: Sci. Appl.* **2020**, *9*, 1−30.
(62) Ma, G.; Xiao, M.; Chan, C. T. Topological phases in acoustic and mechanical systems. *Nat. Rev. Phys.* **2019**, *1*, 281−294.
(63) Lin, M.; Hughes, T. L. Topological quadrupolar semimetals. *Phys. Rev. B: Condens. Matter Mater. Phys.* **2018**, *98*, 241103.
(64) Wieder, B. J.; Wang, Z.; Cano, J.; Dai, X.; Schoop, L. M.; Bradlyn, B.; Bernevig, B. A. Strong and fragile topological Dirac semimetals with higher-order Fermi arcs. *Nat. Commun.* **2020**, *11*, 1−13.
(65) Wang, H.-X.; Lin, Z.-K.; Jiang, B.; Guo, G.-Y.; Jiang, J.-H. Higher-Order Weyl Semimetals. *Phys. Rev. Lett.* **2020**, *125*, 146401.
(66) Slater, J. C.; Koster, G. F. Simplified LCAO Method for the Periodic Potential Problem. *Phys. Rev.* **1954**, *94*, 1498−1524.
(67) Takegahara, K.; Aoki, Y.; Yanase, A. Slater-Koster tables for f electrons. *J. Phys. C: Solid State Phys.* **1980**, *13*, 583.

https://doi.org/10.1021/acs.nanolett.1c02661
Nano Lett. 2021, 21, 7056−7062